JGR Biogeosciences

RESEARCH ARTICLE
10.1029/2024JG008307

# Multiple Elevation-Dependent Climate Signals From Quantitative Wood Anatomical Measurements of Rocky Mountain Bristlecone Pine

**Julie Edwards[1,2,3], Will L. Tintor[4], Alexandre F. Nolin[2,3], Connie A. Woodhouse[2,3], Georg von Arx[5,6], and Kevin J. Anchukaitis[2,3]**

[1]Bren School of Environmental Science & Management, Santa Barbara, CA, USA, [2]Laboratory of Tree-Ring Research, University of Arizona, Tucson, AZ, USA, [3]School of Geography, Development & Environment, University of Arizona, Tucson, AZ, USA, [4]New Mexico Office of the State Engineer Hydrology Bureau, Santa Fe, NM, USA, [5]Swiss Federal Institute for Forest Snow and Landscape Research WSL, Birmensdorf, Switzerland, [6]Oeschger Centre for Climate Change Research, University of Bern, Bern, Switzerland

**Key Points:**

- Quantitative wood anatomy disentangles distinct temperature and moisture signals in Pinus aristata tree rings
- Earlywood lumen area correlates with moisture at low and high-elevation sites, showing potential for drought reconstructions
- Latewood attributes correlate with temperature only at the high-elevation site, with declining climate sensitivity in recent time

**Correspondence to:**
J. Edwards,
julieedwards@arizona.edu

**Citation:**
Edwards, J., Tintor, W. L., Nolin, A. F., Woodhouse, C. A., von Arx, G., & Anchukaitis, K. J. (2025). Multiple elevation-dependent climate signals from quantitative wood anatomical measurements of Rocky Mountain bristlecone pine. *Journal of Geophysical Research: Biogeosciences*, *130*, e2024JG008307. https://doi.org/10.1029/2024JG008307

Received 28 JUN 2024
Accepted 24 DEC 2024

**Abstract** Southwestern North America has experienced significant temperature increases over the last century, leading to intensified droughts that significantly affect montane forests. Although tree-ring data have provided long-term context for this recent drought severity, the varying physiological responses of trees to climate variability make it challenging to disentangle the combined influence of temperature and soil moisture. Here we investigate complex climate-growth relationships in Rocky Mountain bristlecone pine (*Pinus aristata*) at a low-elevation and a high-elevation site using quantitative wood anatomy (QWA). Significant correlations with climate were found for low-elevation tree-ring width (TRW) and earlywood chronologies, including positive correlations with spring and early summer precipitation and drought indices and negative correlations with spring and early summer maximum temperatures. At high elevations, TRW and earlywood chronologies show positive responses to summer moisture, whereas latewood chronologies correlate positively with August and September maximum temperatures and negatively with August precipitation. We leverage this differing seasonality of moisture and temperature signals and compare the QWA data to known droughts. The earlywood lumen area is found to be highly responsive to drought because of its physiological reliance on water availability for maintaining turgor pressure during cell enlargement. We also observed a decline in temperature sensitivity at the high elevation site, suggesting shifts in the dominance of limiting factors. Integrating QWA with traditional dendrochronology improves interpretations of tree-ring data for use in climate reconstruction, offering detailed insights into tree physiological responses and the mix of environmental and developmental controls on cell growth.

**Plain Language Summary** This study investigates the complex relationships between climate variability and tree growth in Rocky Mountain bristlecone pines (*Pinus aristata*) across an elevation gradient using tree-ring wood anatomy. We analyzed 100 years of tree-ring data from two sites in New Mexico, one at a lower elevation and one at a higher elevation. There are distinct climate signals at the two sites. At the lower elevation, ring-width and cell data from the early part of the tree ring show a dominant moisture signal in the months prior to and at the beginning of the growing season. At the higher elevation, trees reflect both moisture and temperature signals during the growing season; early ring-width and cell data show a moisture signal and late ring-width and cell data relate to temperature. Cell size from the early part of the tree ring at both elevations is more sensitive to drought compared to traditional whole-ring measurements. Furthermore, we observed a decline in the temperature sensitivity of wood formation at higher elevations, suggesting shifts in the dominance of the growth limiting factors. These findings emphasize the value of integrating high-resolution wood anatomy data with traditional ring-width measurements for studying forest responses to climate change.

## 1. Introduction

Southwestern North America (SWNA; 30–45°N, 105–125°°W) has experienced a significant temperature increase over the last century (Marvel et al., 2023; Vose et al., 2017). Climate model simulations from Phase 6 of the Coupled Model Intercomparison Project (CMIP6) project intensified droughts in SWNA because of the combination of rising temperatures and vapor pressure deficits and decreasing precipitation in some parts of the region (B. I. Cook et al., 2020, 2021). Already since the beginning of the 21st century, SWNA has experienced

exceptional aridity attributed to a combination of lower precipitation and high temperatures (Mankin et al., 2021; Williams et al., 2022). Warmer temperatures have also affected streamflow (Das et al., 2011; Milly & Dunne, 2020; Udall & Overpeck, 2017; Woodhouse et al., 2016). The severity and duration of the ongoing SWNA megadrought is driven by anthropogenic warming (Williams et al., 2022), underscoring the urgent need to better understand the role of temperature on drought severity in the past, present, and future (B. I. Cook et al., 2021; Griffin & Anchukaitis, 2014; King et al., 2024; Williams et al., 2020).

Tree-ring data in the SWNA region have played a crucial role in providing long-term context for contemporary drought severity and for assessing the influence of anthropogenic climate change (Meko & Woodhouse, 2011; Stahle et al., 2016; Williams et al., 2022). Across the region, numerous tree-ring based reconstructions have been developed to analyze streamflow (Gangopadhyay et al., 2022; Meko et al., 2007; Woodhouse et al., 2006, 2012), precipitation (D'Arrigo & Jacoby, 1991; Griffin et al., 2013; Ziaco et al., 2020), and soil moisture indices (E. R. Cook et al., 2004). Recently, Heeter et al. (2021) developed four regional temperature reconstructions for the western North America temperate zone using the blue intensity tree-ring proxy, spanning approximately 300–400 years to the present. Despite these recent advances, however, the number of temperature reconstructions remains small compared to those for precipitation and soil moisture. Moreover, montane trees across SWNA respond to a range of climate variables, including rainfall, snow, air temperature, soil moisture, and their combined effects (Bunn et al., 2011, 2018; Fritts, 1974; Salzer et al., 2014). The varying and complex physiological responses of trees to climate variability can make it challenging to disentangle or isolate the multiple climate drivers of drought severity through a conventional tree-ring record approach (Tintor & Woodhouse, 2021).

Rocky Mountain bristlecone pine (*Pinus aristata* Engelm.) could provide an additional resource for millennial-scale perspectives on drought frequency, severity, and duration in SWNA (LaMarche Jr & Stockton, 1974; Tintor & Woodhouse, 2021). The Great Basin bristlecone pine (*Pinus longaeva*) has been extensively studied because of its longevity and the preservation of ancient wood remnants (Salzer et al., 2009, 2019); however, a spatially complex mixture of precipitation and temperature signals in this species still complicate their interpretation (Bunn et al., 2011, 2018; Salzer et al., 2014). Previous studies on *Pinus longaeva* have found a shift in the main climatic factor driving tree growth as a function of elevation (Bunn et al., 2018; Salzer et al., 2009). Various methods, including cluster analysis, experimental temperature sensors, and simulated tree-ring growth models, have been used to study and account for these mixed signals (Bruening et al., 2017; Bunn et al., 2018; Tran et al., 2017). In contrast, the Rocky Mountain bristlecone pine (*P. aristata*) has received more limited investigation for climate reconstruction and only a few precipitation and temperature reconstructions have been developed (Routson et al., 2011; Salzer & Kipfmueller, 2005; Tintor & Woodhouse, 2021; Woodhouse et al., 2011). Recent research by Tintor and Woodhouse (2021) identified a complex climate response in *P. aristata* ring-width chronologies, including a drought stress signal in June and a positive minimum temperature response in late summer. The presence of multiple climate responses across the geographic range of *P. aristata* emphasizes the need for caution when using this species in regional climate reconstructions (Tintor & Woodhouse, 2021); however, a more nuanced understanding of the climate signals present in *P. aristata* could enhance its potential as a long-term climate record and provide new information on the coupled hydroclimate and temperature history of SWNA.

Our research objective here is to investigate the response of *P. aristata* to climate variability and change over the last century in SWNA and identify the potential implications for climate reconstruction. Therefore, we focus on two stands of *P. aristata* located at the species's upper and lower treeline near its southern limit in the Rocky Mountains to investigate the climate signals in this species and understand the impact of drought and rising temperatures on tree-ring growth. This experimental design is motivated by the findings of Salzer et al. (2009), who observed that tree-ring width (TRW) transitions from moisture-limited at lower elevations to more temperature-limited at higher elevations. However, because of increasing temperatures and the early 21st century megadrought, these elevation thresholds are changing, resulting in forests becoming more moisture-limited even at higher elevations (Salzer et al., 2009). Investigating the same species at upper and lower treeline therefore provides a natural laboratory to observe how increasing temperatures affect tree growth. Here we use quantitative wood anatomy (QWA) to disentangle the connections between climate and annual ring formation in *P. aristata* trees that have been shown to have a mixed climate signal in their annual ring-width increments. QWA measurements can potentially provide more detailed information about intra-seasonal and multivariate climate signals than can be detected in TRW data alone. QWA provides cellular-scale measurements which have a well-understood biological and functional foundation, permitting an analysis of the mechanistic link between

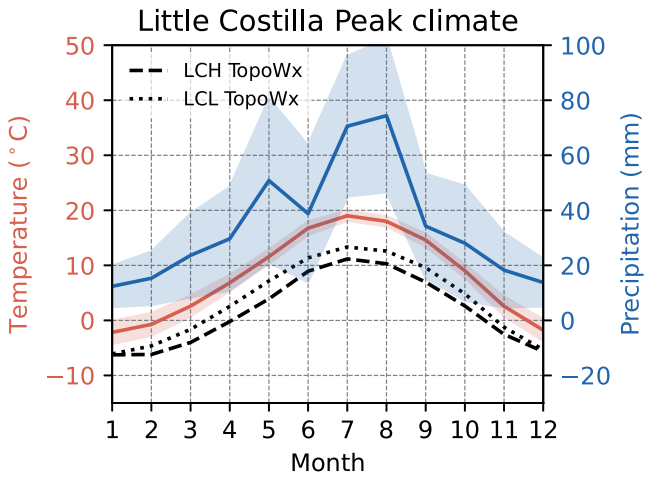


**Figure 1.** Climatology of Little Costilla Peak grid cell from CRU TS Version 4.06 data set (Harris et al., 2020) averaged over the 1901–2021 period. Shaded envelopes show ±1 standard deviation of the monthly mean. Blue line depicts CRU precipitation, red line depicts CRU temperature, and the black dashed and dotted line respectively depict average TopoWx ("Topography Weather") temperature at LCH and LCL sites.

climate and growth response (Björklund et al., 2020; Hacke et al., 2001; Seftigen et al., 2022), with potential for analysis of the multivariate controls on tree growth (Carrer et al., 2017; Cuny et al., 2014; Fonti et al., 2010). Only two other QWA studies exist for the SWNA region, one using *Pseudotsuga menziesii* from eastern Arizona (Balanzategui et al., 2021), and the other using *Pinus longaeva* from eastern Nevada (Ziaco, Biondi, & Heinrich, 2016). This study provides the first QWA analysis of *P. aristata*, providing an innovative approach for disentangling the complex climate signals in its growth, with implications for improving long-term paleoclimate reconstructions in the SWNA region.

## 2. Data and Methods

### 2.1. Study Sites

We use living *P. aristata* samples from two sites at Little Costilla Peak: Little Costilla Peak Low (LCL; 2,900 m, 36.78°N, 105.24°W) and Little Costilla Peak High (LCH; 3,600 m, 36.82°N, 105.22°W). The collection of these samples is described in Tintor and Woodhouse (2021). Little Costilla Peak is located in the Southern Rocky Mountains ecoregion, which is characterized by dramatic variation in topography, winter-time temperature inversions in valleys, and a snow-dominated precipitation regime with a dry spring interstitial period (Wiken et al., 2011). Mean temperatures at the CRU 0.5°x0.5° grid cell closest to Little Costilla Peak (Harris et al., 2020) are above freezing for most of the year and July and August see the highest precipitation amounts (Figure 1). LCH trees were collected from east-aspect slopes and LCL trees were sampled on the valley floor. *P. aristata* trees at Little Costilla Peak are in the southernmost portion of their estimated range and are within the elevation range (between 2,700 and 3,700 m) at which *P. aristata* is commonly found (Schoettle & Coop, 2017).

### 2.2. Quantitative Wood Anatomy

For QWA analysis, eight trees were selected from LCL which had an average age of 198 years, and 10 trees from LCH which had an average age of 201 years. Dating of these trees was confirmed using previous TRW measurements from Tintor and Woodhouse (2021) prior to processing the cores for QWA analysis. We cut the wood samples to a thickness of 10 µm using a rotary microtome (Microm HM355S). The wood microsections were stained with a safranin solution, permanently fixed in Eukitt, and prepared after standard procedures (Gärtner & Schweingruber, 2013; von Arx et al., 2016). Digital images of the microsections were produced at the Swiss Federal Research Institute WSL in Birmensdorf, Switzerland, using a Zeiss Axio Scan Z1. We measured the cell-lumen area, cell-wall thickness, and cell-wall area for the period 1917–2017 on all samples using the ROXAS (v3.1) image analysis software (von Arx & Carrer, 2014; Prendin et al., 2017). We excluded annual measurements of samples with cell walls that had been damaged during sampling or preparation. We aggregated cell measurements into consecutive 20 µm wide bands within each annual ring and used the 75th percentile of cell measurements within each band, to create intra-annual measurement profiles of anatomical traits. The 75th percentile was chosen to reduce the effect of outliers; for detailed methodology of dendroanatomical measurements and data processing, see Björklund et al. (2020). From these aggregate measurements, we created annual chronologies for multiple cell characteristics. Maximum parameters (e.g., maximum radial cell-wall thickness (MxRCWT)) were determined by identifying the highest values along the intra-annual profile for each measured trait. The width of earlywood and latewood was determined after separating the two tissues using a Mork's index of 1 (Denne, 1989; Mork, 1928). Earlywood lumen area (EWLA) is the mean cross-sectional lumen area of cells within the earlywood for each ring. We calculated anatomical maximum latewood density (aMXD) as the maximum ratio between the cell wall area and the total cell area (the sum of the cell wall area and cell lumen area) for any given year (Figure 2).

After E. R. Cook et al. (2017), any missing annual values in the cell characteristic series were filled prior to detrending. We used a linear interpolation to fill missing values, then each series was detrended using a 30-year cubic spline. We then removed the infilled values before averaging at the site level using a Tukey's biweight

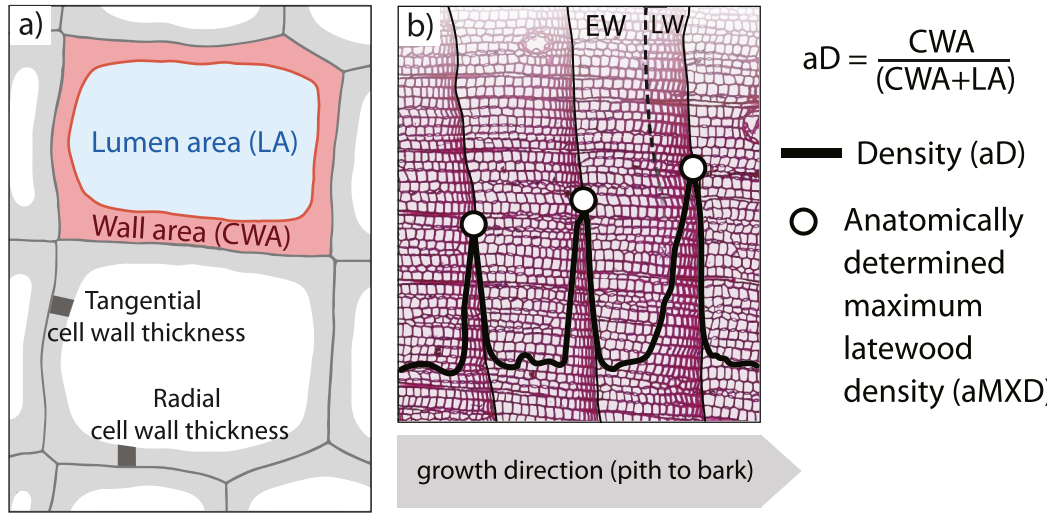


**Figure 2.** Illustration of the wood cell measurements used in this study: radial cell-wall thickness, tangential cell-wall thickness, lumen area and cell-wall area. Anatomical density (aD) of each cell is defined as the ratio of cell-wall area to overall cell area (sum of wall and lumen area) (a). Exemplary intra-annual profiles for aD (black curve). Maximum values for aD (circles) are extracted for each ring to obtain annual anatomically determined maximum latewood density (aMXD). Earlywood lumen area (EWLA) was obtained by averaging the lumen area values of cells located in the earlywood (EW) (b). Figure adapted from Björklund et al. (2021).

robust mean (Bunn, 2008). This detrending method was chosen to focus on the inter-annual variability associated with climate controls on growth, rather than long-term trends. The mean inter-series correlation coefficient (rbar) for each cell characteristic chronology was calculated as the mean correlation coefficient between all combinations of different series pairs (Bunn, 2008). The expressed population signal (EPS) was used to assess the common signal between series and is a function of the rbar and the number of series used (Wigley et al., 1984).

Although a large number of measurements and their derivatives are available from QWA, here we selected specific measurements to further analyze based on rbar values that indicated good between-series agreement, as well as those used in other QWA studies (Björklund et al., 2020; Seftigen et al., 2022). These include: total TRW, earlywood width (EWW), latewood width (LWW), earlywood lumen area (EWLA), maximum tangential cell-wall thickness (MxTCWT), MxRCWT and anatomically determined maximum latewood density (aMXD) (Figure 2). To investigate similarities between cell characteristic chronologies, we performed principal component analysis (PCA). Chronologies were first normalized and scaled to the same mean and variance and then PCA was performed on the correlation matrix. The first two modes were then rotated using varimax rotation (Richman, 1986).

### 2.3. Climate Analysis

We extracted monthly precipitation and maximum temperature from the CRU TS Version 4.06 (Harris et al., 2020) and the Standardized Precipitation-Evapotranspiration Index (SPEI; Beguería et al., 2014) for the 0.5°x0.5° grid cell corresponding to Little Costilla Peak, which covers both LCL and LCH sites (36.5°N–37.0°N, 105.0°W–104.5°W, 1901–2021). We used SPEI as a drought index, as the combination of standardized anomalies of precipitation and potential evapotranspiration can be used to represent the timing, duration, and severity of soil moisture deficits. To assess the temperature climatology differences across elevation, we used Topography Weather (TopoWx) daily climate data for both LCL and LCH spanning 1948–2016 (Oyler et al., 2016). Although it covers a shorter time span, TopoWx data has a higher spatial and temporal resolution and explicitly accounts for the elevation difference between the LCL and LCH sites. This data was only used to assess the average difference in absolute temperature across LCL and LCH. Finally, we also acquired monthly snow water equivalent (SWE) data from the Red River Pass SNOTEL site (3,000 m, 36.7°N, 105.33°W) for the 1981–2017 water years (USDA Natural Resources Conservation Service, 2024).

**Table 1**
*Mean Inter-Series Correlation Coefficient Rbar, Expressed Population Signal (EPS), and First-Order Autocorrelation (AR1; *$p < 0.05$) Values for Detrended Tree-Ring Widths and Cell Characteristic Chronologies, Based on the Common 1917–2017 Period*

| Chronology | LCL rbar ($n = 8$) | LCL EPS | AR1 | LCH rbar ($n = 10$) | LCH EPS | AR1 |
|---|---|---|---|---|---|---|
| TRW | 0.45 | 0.87 | 0.40* | 0.40 | 0.87 | 0.32* |
| EWW | 0.45 | 0.87 | 0.38* | 0.42 | 0.88 | 0.33* |
| EWLA | 0.44 | 0.86 | 0.13 | 0.30 | 0.81 | 0.18 |
| LWW | 0.30 | 0.78 | 0.15 | 0.38 | 0.86 | −0.35* |
| MxTCWT | 0.29 | 0.77 | 0.09 | 0.31 | 0.82 | −0.17 |
| MxRCWT | 0.26 | 0.73 | 0.03 | 0.38 | 0.86 | −0.39* |
| aMXD | 0.21 | 0.68 | −0.13 | 0.35 | 0.84 | −0.28* |

*Note.* Chronologies reported: total tree-ring width (TRW), earlywood width (EWW), latewood width (LWW), earlywood lumen area (EWLA), maximum tangential cell-wall thickness (MxTCWT), maximum radial cell-wall thickness (MxRCWT) and anatomically determined maximum latewood density (aMXD).

We calculated Pearson correlation coefficients between monthly climate data and the wood cell characteristic chronologies at each site for the full period of our QWA data (1917–2017). The climate data were first detrended using a 30-year cubic spline curve to provide a spectrally similar comparison to the cell characteristic chronologies and emphasize interannual controls on ring formation (Ols et al., 2023). Correlations between the QWA data and SWE data were calculated for their period of common overlap (1981–2017).

To understand how the QWA cell characteristic chronologies capture different drought dynamics, we selected three anatomical chronologies with the highest correlation coefficient with climate (see Results). We scaled these three chronologies using the Composite Plus Scale (CPS; Jones & Mann, 2004) method. The CPS method scales the tree-ring data to the mean and standard deviation of the observational climate data during an overlapping calibration period. In climate reconstructions, the fit between the scaled tree-ring data and the observational climate data is typically evaluated for a validation period of withheld observational data. Here, we first scaled the mean of the LCH aMXD and MxRCWT (aMXD/MxRCWT) to the average of the August and September maximum temperatures. Second, we scaled the LCL EWLA to spring (March through June) average SPEI. Finally, we scaled the LCH EWLA to June and July average SPEI. The full period was used to scale the proxy data to its respective climate index. We calculated Pearson correlation coefficients between the climate indices and the scaled proxy data over the full analysis period (1917–2017), an early period (1917–1967), and a late period (1967–2017). The full period of the cell chronologies overlaps with four well-known historic drought periods, which we use to evaluate the ability of QWA data to capture the features of droughts with varying characteristics and drivers. These include the 1930s Dust Bowl drought which can be considered a "proto hot-drought" (a heat-amplified drought characterized by high temperatures combined with low precipitation) (B. I. Cook et al., 2009), the 1950s Southwest drought which is a more typical drought caused by La Niña-like conditions, and the 21st century anthropogenic megadrought, which includes two distinct drought periods we analyze separately: the early 2000s and the 2011/2012 drought years.

## 3. Results

### 3.1. Common Signals in Chronologies

Overall, the individual chronologies demonstrate robust common signals (rbar ≥ 0.30), with the exceptions of MxTCWT, MxRCWT, and aMXD at the lower elevation LCL site (Table 1). We observe that the TRW time series generally have slightly higher rbar and EPS values than the cell characteristic chronologies at both sites. Earlywood cell characteristics chronologies (TRW, EWW, and EWLA) have higher rbar values at low-elevation LCL than high-elevation LCH, whereas the latewood cell characteristics chronologies (MxTCWT, MxRCWT, and aMXD) have higher rbar values at LCH (Table 1). None of the cell characteristic chronologies have significant ($p < 0.05$) positive lag-1 autocorrelation at either site, but the latewood-related chronologies (LWW, MxRCWT, aMXD) at LCH have significant negative lag-1 autocorrelation. TRW and EWW have significant

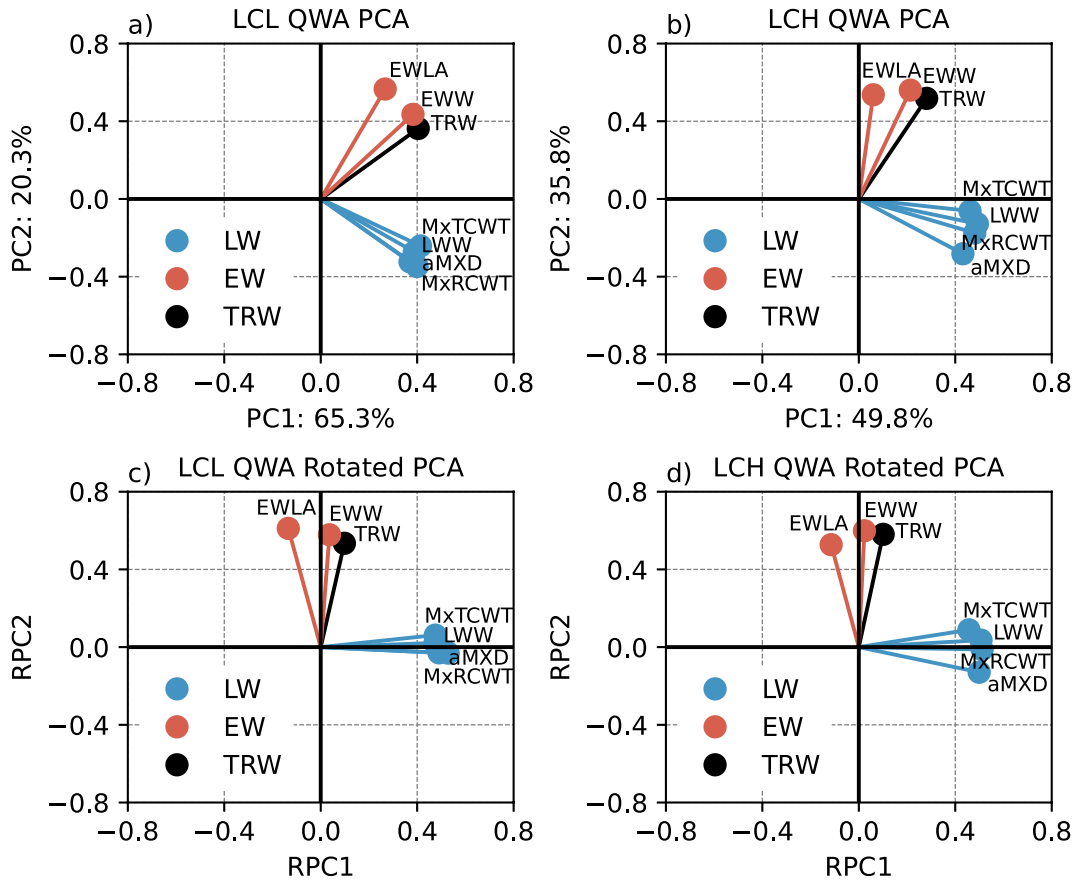


**Figure 3.** Biplot of the first two principal components of the principal component analysis performed over the 1917–2017 period on the tree-ring width (TRW) and cell characteristic chronologies, unrotated (a, b) and varimax rotated (c, d). The colors of the vectors correspond to the cell characteristic's location in the overall ring (LW: latewood, EW: earlywood, TRW: total TRW). The first two components together represent 85.6% of the total variance at LCL (a), and 85.6% of the total variance at LCH (b).

positive lag-1 autocorrelation at both sites (Table 1). The mean ring width during the 1917–2017 study period was 782 μm for LCL and 752 μm for LCH.

The co-variability between the various TRW and cell characteristic chronologies over the common 1917–2017 period at LCL and LCH was assessed through PCA. Similar loading patterns for the chronologies as well as the percentage of total variance explained by each mode of covariability were found for the LCL and LCH sites. At LCL, PC1 explains 65.3% of the variance and PC2 explains 20.3% of the variance (85.6% of the total variance). The magnitude of the loading on PC1 is similar for both latewood and earlywood chronologies. On PC2, the loading discriminates between the latewood and earlywood chronologies, with TRW, EWW, and EWLA grouping together and LWW, MxTCWT, MxRCWT, and aMXD all showing the opposite sign (Figure 3a). Applying the varimax rotation further emphasizes the clustering of the latewood chronologies on rotated PC1 (RPC1), and the earlywood chronologies and TRW grouping together on rotated PC2 (RPC2; Figure 3c). Similar results are found for the data from LCH. The first two components there together capture 85.6% of the total variance across all chronologies from the site, although the explained variance is more equitable at LCH than LCL, with PC1 explaining 49.8% and PC2 explaining 35.8%. Once again, loadings for the latewood chronologies cluster together in the bivariate plot and are differentiated from earlywood chronologies and TRW (Figure 3b). For the rotated PCs at LCH, similar to LCL, the latewood chronologies are isolated on RPC1 and the earlywood chronologies on RPC2 (Figure 3d).

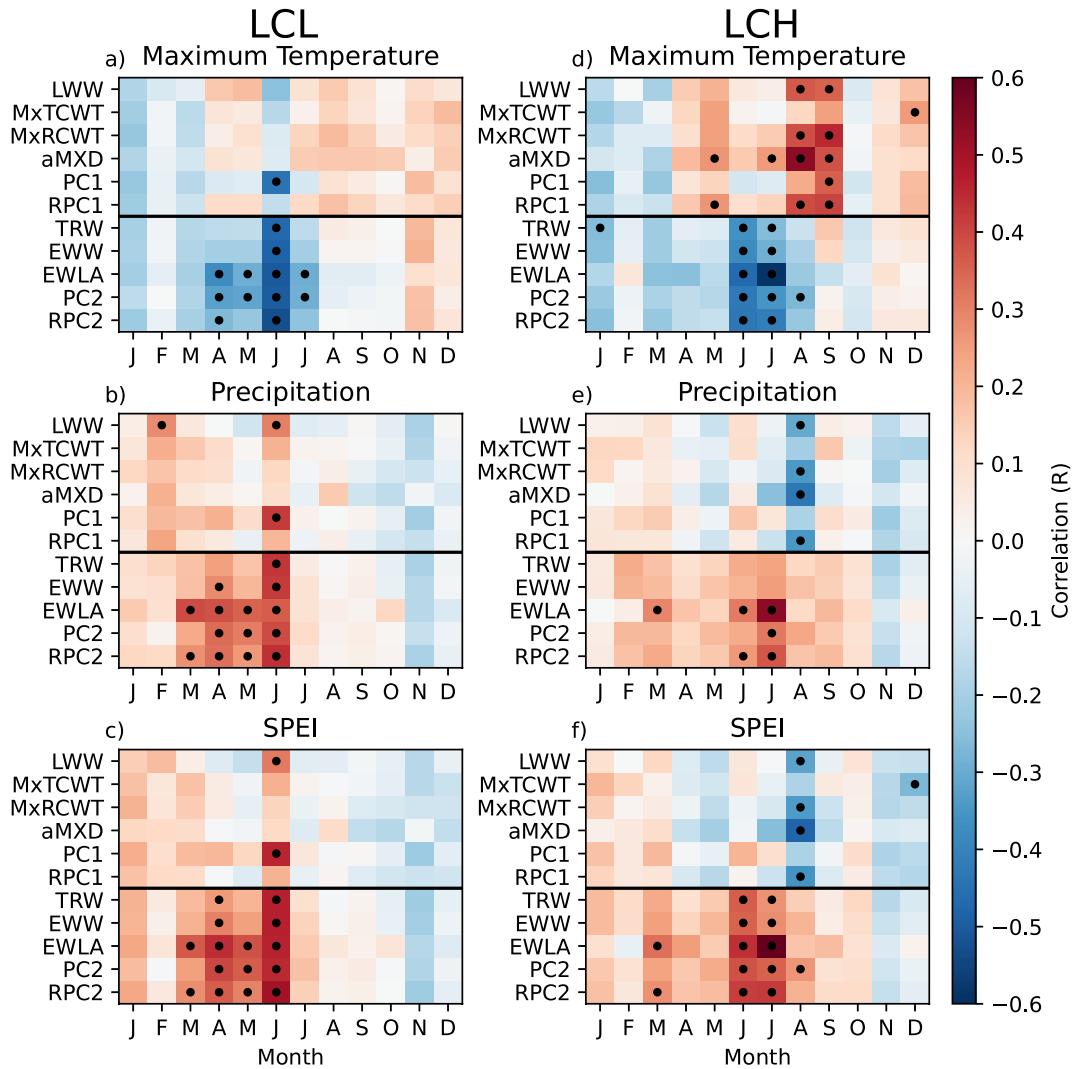


**Figure 4.** Pearson correlation results between the tree-ring width and cell characteristic chronologies, and the first two (R)PC time series, at LCL (a, c, e) and LCH (b, d, f) and monthly climate data: maximum temperature (a, b), precipitation (c, d), and SPEI (e, f) and for 1917–2017. Dots indicate significant ($p < 0.01$) correlation.

### 3.2. Climate Analysis

Climate correlations across the chronologies and their PCs and RPCs differ between LCL and LCH sites, with trees from LCL demonstrating a dominant moisture signal in the months prior to and then at the beginning of the growing season, whereas trees from LCH reflect a combined moisture and temperature signal largely during the growing season itself (Figure 4). Differences in the climate response are also observed for ring-widths versus cell chronologies, as well as between earlywood and latewood chronologies. Earlywood chronologies tend to demonstrate a more moisture-related signal whereas the latewood chronologies are more consistently related to temperature.

At LCL, very few meaningful climate signals were found for the latewood chronologies that loaded together on RPC1 (LWW, MxTCWT, MXRCWT, and aMXD), with the only significant ($p < 0.01$) correlations observed between LWW and Feb and June precipitation and June SPEI. Conversely, we find significant correlations with climate for LCL's PC1, PC2, RPC2, TRW, and various earlywood chronologies. At LCL these include positive correlations with spring and early summer precipitation and SPEI, and negative correlations with spring and early summer maximum temperatures. EWLA correlates with March through June precipitation and SPEI at LCL, which drives the same sensitivity for RPC2 and PC2 (to a lesser extent). April SPEI also weakly correlates with

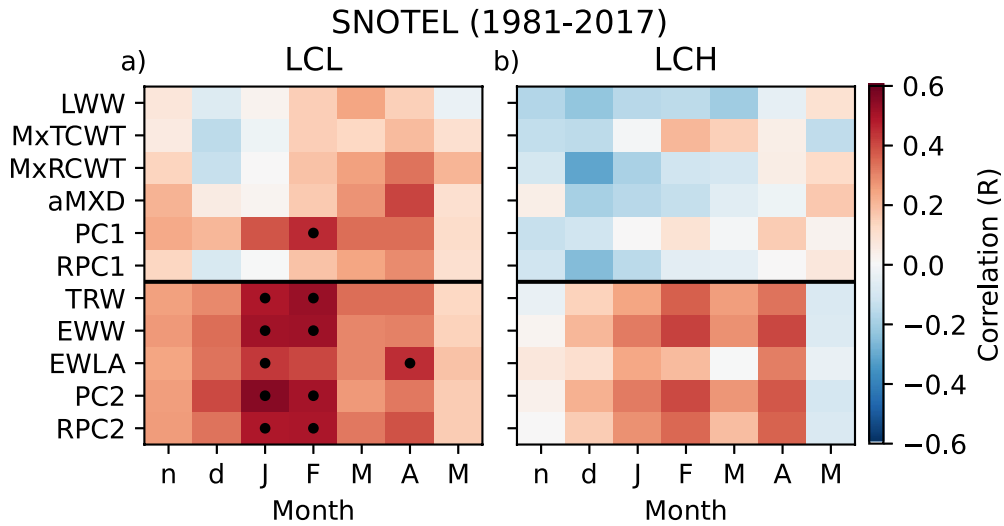


**Figure 5.** Pearson correlation results between the tree-ring width and cell characteristic chronologies and the first two (R)PC time series, at LCL (a) and LCH (b), and Red River Pass SNOTEL snow water equivalent data for 1981–2017 water years. Dots indicate significant ($p < 0.01$) correlation.

TRW and EWW. At LCL, the most negative correlation ($r = -0.53$) for a single month is between RPC2 and June maximum temperature (Figure 4a) and the most positive correlation ($r = 0.51$) is between RPC2 and June SPEI (Figure 4e).

At LCH, two different signals emerge across the various chronologies. As also observed at LCL, the earlywood chronologies, TRW, PC2, and RPC2 show positive responses to moisture, although at this higher elevation site they are largely confined to summer. A strong correlation is observed between EWLA and July precipitation, and SPEI. The latewood width and cell chronologies (except MxTCWT), as well as RPC1 on which they load, correlate positively with August and September maximum temperature, and negatively with August precipitation and SPEI. At LCH, The most negative correlation ($r = -0.59$) for a single month is between EWLA and July maximum temperature (Figure 4b) and the most positive correlation ($r = 0.61$) is between EWLA and July SPEI (Figure 4f).

Correlations between the Red River Pass SWE and LCL chronologies demonstrated significant ($p < 0.01$) positive correlations between January and February SWE and the TRW, EWW, and related (R)PC chronologies (Figure 5a). The LCL EWLA chronology showed a weaker association to January and April SWE. There is no significant correlation between SWE and any of the latewood chronologies. The strongest correlation ($r = 0.55$) for a single month is between PC2 and January SWE. There is no significant ($p < 0.01$) correlation with SWE at LCH, although the positive sign of the association between TRW and the earlywood chronologies is the same as at the lower site (Figure 5b).

To understand how the QWA cell characteristic chronologies capture drought dynamics we used the climate-scaled data for the three strongest associations found between tree-ring chronologies and climate at both sites (Figure 4). As described in above, these are the August and September average maximum temperature and the LCH aMXD and MxRCWT averaged together (aMXD/MxRCWT); the March through June average SPEI and LCL EWLA; and the June and July average SPEI and LCH EWLA.

The correlation coefficients for the early period (1917–1967) are generally higher than the late period (1967–2017) across all the metrics. This decrease in the strength of the correlation from the early to the late period is most pronounced however for the August/September maximum temperature series (Table 2).

**Table 2**
*Pearson Correlation Coefficient (r) Values for Correlation Between Observed Climate Values and Corresponding Scaled Proxy-Data Across the Full Analysis Period As Well As Subdivided Into Early (1917–1967) and Late (1967–2017) Periods.*

| Climate index | (1917–2017) *r* | (1917–1967) *r* | (1967–2017) *r* |
|---|---|---|---|
| Aug/Sep max. temperature | 0.52 | 0.65 | 0.44 |
| March–June SPEI | 0.64 | 0.67 | 0.63 |
| June/July SPEI | 0.66 | 0.69 | 0.66 |

*Note*. These Correlations Include Aug/Sep Maximum Temperature and LCH aMXD/Maximum Radial Cell-Wall Thickness, March–June SPEI and LCL EWLA, and June/July SPEI and LCH EWLA. All Correlations Are Significant ($p < 0.01$)

## 4. Discussion

### 4.1. Environmental and Developmental Controls on Cell Formation

Our results show that there are distinct external environmental and internal developmental controls on cell growth across sites, and between earlywood versus latewood chronologies. LCL is a more typical SWNA moisture-limited site where the earlywood chronologies have a robust moisture-limitation signal (Figure 4). In contrast, the latewood chronologies at LCL appear to contain relatively few significant correlations with climate and therefore may be more strongly influenced by endogenous developmental controls, such as programmed cell death, hormonal variations, and the evolutionary phenological processes that govern cell-wall thickening and latewood formation (Buttò et al., 2020; Rathgeber et al., 2016). The minor role of climate in determining variability in these features may also account for the reduced rbar observed in the latewood chronologies (Table 1). At LCH, however, there is a coherent environmental control on the latewood variables, suggesting temperature variations have a more uniform and significant influence on the processes of latewood formation in a higher elevation environment (Cuny & Rathgeber, 2016; Cuny et al., 2019). The variance explained across all the width and anatomical chronologies is also more evenly split between PC1 and PC2 at LCH (Figure 3b), which implies a more balanced influence of growth drivers across both earlywood and latewood, likely explained by the two distinct climate signals present in those chronologies (June–July precipitation and SPEI, August–September maximum temperature, Figure 4).

The underlying internal physiology of wood cells ultimately explains the existing climate signals in the cell characteristic chronologies, as the timing and nature of wood formation directly reflect the tree's response to environmental conditions each year (Fonti et al., 2010; Fritts, 1976; Vaganov et al., 2006). QWA data can provide multiple climate signals because it is able to capture the results of distinct cell growth processes: cell division which controls the number of cells in a ring, cell expansion which controls variations in lumen area, and cell-wall thickening, which controls the cell-wall thickness and the majority factor of aMXD (Fritts, 1976; Rathgeber et al., 2016; Vaganov et al., 2006, 2011). Wood cell anatomy and the cell expansion process is highly adaptive to hydroclimate as a drought-resistance and hydraulic safety strategy (Fonti et al., 2010; Guérin et al., 2020; Hacke et al., 2001; Lauder et al., 2019; Olano et al., 2012; Pittermann et al., 2006). EWLA, for example, is intrinsically linked to the stem's hydration state during cell formation, with water availability being critical for maintaining sufficient turgor pressure throughout the cell enlargement phase (Balanzategui et al., 2021; Cabon et al., 2020; Peters et al., 2021; Vaganov et al., 2006). Cell-wall thickening in the earlywood provides wood structural support to minimize cavitation (Hacke & Sperry, 2001), whereas cell-wall thickening in the latewood provides wood structural support to stabilize the trunk. The cell-wall thickening process is also related to carbon fixation and carbohydrate mobilization, which are limited by temperature at treeline sites (Hoch & Körner, 2012).

The inherent interconnectedness of environmental and developmental controls on cell growth contributes to the complexity of interpreting tree-ring data for climate reconstructions, necessitating the consideration of the underlying physiological mechanisms of cell growth and their seasonal timing when using QWA data. Because Little Costilla Peak is located at the southernmost part of the estimated range for *P. aristata* (Schoettle & Coop, 2017), it is more likely to contain a moisture signal (even at higher elevations) and the potential for a pure temperature reconstruction is more limited. However, this means it is a useful location for detecting potential multivariate climate thresholds and allows added value from a QWA approach. QWA data can provide intra-seasonal climate signals, as successive tracheid rows through an annual ring can reflect distinct climate signals throughout the growing season (Balanzategui et al., 2021; Castagneri et al., 2017). Additionally, the strong influence of drought on EWLA suggests that anatomical variables can provide different and stronger climate information than traditional ring-width variables alone, enhancing the potential for more accurate drought reconstructions, especially at sites with a mixed climate signal (Martin-Benito et al., 2013). The onset of wood formation, influenced by various environmental factors including temperature, plays a vital role in understanding climate-growth relationships, which is crucial for accurate dendroclimatic reconstructions (Gruber et al., 2009; Vaganov et al., 2006; Ziaco, Biondi, Rossi, & Deslauriers, 2016). In-depth studies on cambial physiology, especially for species like *P. aristata*, are essential to unravel the specific environmental factors dictating wood

anatomical growth. Such investigations could involve intensive cambial phenology xylogenesis studies, providing a more detailed understanding of how temperature and other climatic variables affect the growth cycle annually (Ziaco, Biondi, Rossi, & Deslauriers, 2016).

### 4.2. Multiple Climate Signals and Moisture Dynamics

Differences in tree-growth responses to climate variables are evident in our comparative analyses of moisture and temperature signals across elevations. At lower elevations (LCL), growth is primarily moisture-limited, encompassing dual cool and warm-season hydroclimate signals (Figures 4 and 5). These signals are also consistent with how moisture availability can influence wood anatomy. In response to extreme drought conditions, earlywood can show a reduction in cell sizes, potentially a physiological trade-off between hydraulic efficiency and safety (Fonti et al., 2010; Hacke et al., 2001; Han et al., 2023; Olano et al., 2012; Pittermann et al., 2006), although the mechanistic basis and universality of the safety–efficiency trade-off remains debated (Gleason et al., 2016). In contrast, wet conditions lead to the formation of cells with larger lumen, thereby increasing hydraulic conductivity (González-Cásares et al., 2019). Warm and dry summers have been found to reduce ring width and tracheid dimensions in both earlywood and latewood, underscoring the climatic limitations on tree growth during these critical periods of the growing season (Martin-Benito et al., 2013). The SWE signal at LCL (Figure 5) suggests that lower elevation sites, where temperature is less of a constraint on growth, are more sensitive to moisture provided by spring snowmelt.

The high elevation LCH site exhibits a different climatic response (Figures 4d–4f). Here, warm-season signals dominate, with an additional positive temperature signal — in this case in the latewood metrics—that is absent at lower elevations (Bunn et al., 2018; Salzer et al., 2009). This elevation-dependent temperature influence aligns with the findings of Martin-Benito et al. (2013) in Mediterranean forests, who observed that latewood, typically formed in the warmer part of the growing season, is more responsive to summer climate conditions. At LCH, the combination of shorter growing seasons and cooler temperatures makes temperature a critical factor. In contrast, latewood chronologies at LCL exhibit no climate sensitivity, suggesting that the growth processes toward the end of the season at lower elevations are predominantly driven by endogenous factors (Rathgeber et al., 2016) and/or consistent environmental or phenological cues (Cuny & Rathgeber, 2016). Although the LCH temperature signal also reflects covarying moisture dynamics through the temperature-precipitation inverse relationship (Figures 4b and 4d) and possibly land surface feedbacks, we interpret the positive September temperature signal as independent of these, as it is not consistent with coeval hydroclimate variables (Figures 4d–4f).

At LCL, soil moisture dynamics driven by factors including snowmelt and precipitation likely play a crucial role in shaping tree-growth patterns. In mountain ranges of the western United States, the snowpack contributes to the determination of soil moisture at the beginning of the growing season, subsequently influencing the amount of water available for the resumption of cambial processes (Balanzategui et al., 2021; Coulthard et al., 2021), and it has been shown in other mountain environments that this reliance on snow as a fundamental water source extends into the following months (Castagneri et al., 2015). The positive correlation observed between TRW and January and February SWE in recent periods (Figure 5), along with the correlation between EWLA and spring temperature and hydroclimate signals (Figures 4a, 4c, and 4e), suggests that trees use moisture originating from snow during growth initiation (Bailey et al., 2023; Balanzategui et al., 2021; Castagneri et al., 2015). Although both use snow water, TRW (which reflects total cell number formed during the entire growing season) and EWLA (which reflects influences on cell dimensions during the early growing season) "access" this moisture at different times in the growing season because of the staggered timing of the respective growth processes. Bailey et al. (2023) also show that conifers in semi-arid environments under a bimodal precipitation regime can access water originating from winter snowmelt and non-snow water arriving during the summer monsoon. TRW is likely to reflect a complex and integrated signal: at the beginning of the growing season, cell division may be set by the moisture availability from snowmelt (which is itself set by climate conditions before the growing season begins), but it is then modified by non-snow water available in June when the growing season is already well underway (Figure 1). EWLA is initially influenced by some snowmelt from the snow originating in the winter, then is subsequently modulated by any spring precipitation (either as snow or rain), to which it can actively respond. In the study by Ziaco, Biondi, Rossi, and Deslauriers (2016) on higher elevation Great Basin bristlecone, the authors show that the initiation of growth there typically occurs in June. Given the timing for this similar species and the LCL site climatology, it is reasonable to assume that tree growth at LCL commences earlier.

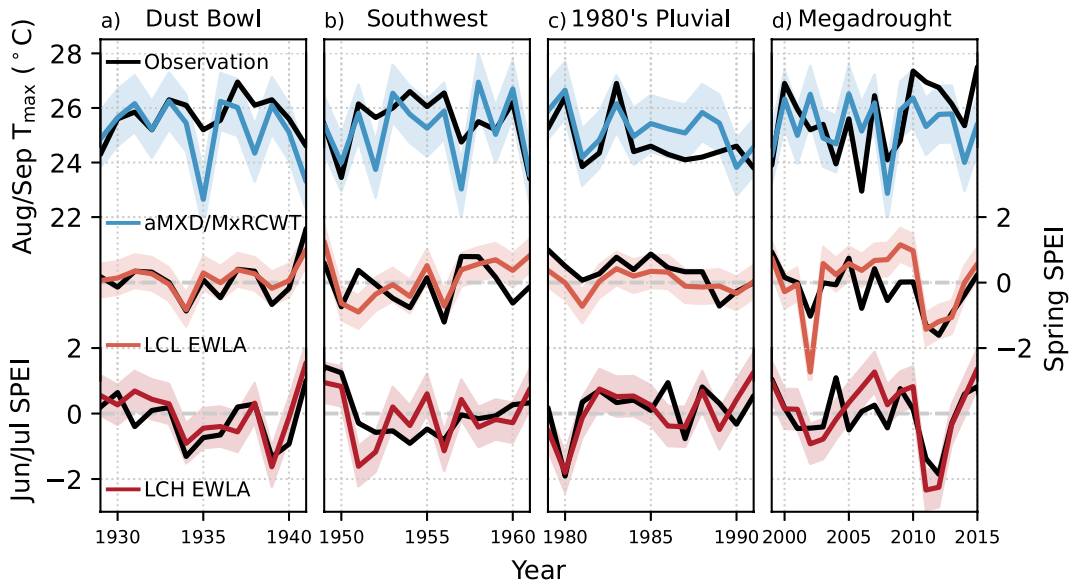


**Figure 6.** Comparisons between selected Composite Plus Scale tree-ring chronologies and climate index. Observation (black): August/September maximum temperature, March–June spring SPEI, and June/July SPEI, and full calibration period scaled proxy data: LCH aMXD and maximum radial cell-wall thickness averaged together (aMXD/MxRCWT; blue), LCL EWLA (light red), LCH EWLA (dark red) time series for the exemplary drought periods and pluvial: Dust Bowl (a), southern Great Plains/Southwest drought (b), the 1980s' pluvial (c), and the 21st century megadrought (d). Shaded envelopes show the root mean square error of the proxy data scaling.

There are a few limitations with the available SWE data in this study. At LCL, correlations of TRW and EWW to non-SWE climate data, which span more years, only show April/June moisture sensitivity without a winter moisture signal (Figures 4a–4c). Either the SWE control on TRW and EWW is more recent, and ring width was not previously limited by SWE, or the data used in the long-term correlation analysis do not capture the snowmelt soil moisture dynamics as accurately as SWE data. At LCH, we find no significant correlations with SWE during the period when snow data are available and trees at the site apparently have a warm-season signal only. However, it is possible that SWE measured at a low elevation like the Red River SNOTEL site may not be representative of the variability in snowpack occurring at the higher elevations of LCH (distance to SNOTEL station 17 km, delta elevation +600m). Differences in topography, such as elevation, aspect, and slope, between LCL, LCH, and the Red River SNOTEL site will lead to variations in snow behavior across these sites, as topography affects snow accumulation and melt dynamics (Jost et al., 2007). It is worth noting that whereas the earlywood/TRW correlations with SWE at LCH are weak, they are in the same positive direction as the significant earlywood/TRW correlations with SWE at LCL. It is possible the correlations with SWE at LCH were significant in the past, but recent enhanced and earlier spring warming lead to non-stationary SWE signals (Coulthard et al., 2021). LCH could have also previously acted as an energy-limited site, with growth having a negative relationship to SWE (Coulthard et al., 2021); however, the short temporal length of SWE data prevent us from making conclusive determinations.

### 4.3. Drought Impacts

QWA data allow us to link seasonal-scale limiting factors to the physiological mechanisms behind distinct xylem cell characteristics. The SPEI observations and scaled EWLA both show known periods of exceptional hydroclimate in the SWNA region (Figure 6), illustrating EWLA's sensitivity to drought conditions via the importance of water availability in the cell expansion process (Balanzategui et al., 2021; Cabon et al., 2020; Peters et al., 2021; Vaganov et al., 2006). EWLA at both LCL and LCH are more than one standard deviation lower than average in the worst years of both the 1930s Dust Bowl and the 1950s Southwest drought: 1934 (E. R. Cook et al., 2007, 2014) and 1956 (E. R. Cook et al., 2007; McGregor, 1985) respectively. In the 21st century, LCL EWLA appears to have had an exaggerated response (−4.6 standard deviations; Figure 6d) in 2002, which was the most severe drought year in the first decade of the 21st century (E. R. Cook et al., 2010). In the record-setting

2011/2012 drought years (Grigg, 2014), LCL EWLA is −2.4 and −2.0 standard deviations in those years, and LCH EWLA is −3.1 and −3.0 standard deviations. QWA data can also be used to identify climate anomalies occurring at specific times during the growing season. For instance, The Dust Bowl drought was characterized predominantly by low summer precipitation, whereas winter precipitation remained closer to the long-term average (E. R. Cook et al., 2007; Kim, 2002). Both the observational June/July average SPEI and the scaled LCH EWLA chronologies show lower values compared to March–June average SPEI (Figure 6a), reflecting this drought's particular seasonality. In 2002, moisture availability during the summer monsoon in central New Mexico and southeastern Arizona helped to offset the warmer temperatures, resulting in observational June/July average SPEI and LCH EWLA (Figure 6d) that are not as low as the LCL EWLA and observational SPEI from earlier in the year (Weiss et al., 2009). In contrast, the low values in the EWLA chronologies at LCL and LCH in 2011 and 2012 indicate a high evapotranspiration demand throughout spring and summer.

We can also use drought periods during which the positive relationship between aMXD/MXrCWT and August/September maximum temperature breaks down to attempt to understand how aridity can affect these cell characteristics. In both the Dust Bowl and the Southwest drought, scaled aMXD/MxRCWT fails to capture anomalously high August/September maximum temperature in the year after the "worst year" of each drought. Scaled aMXD/MxRCWT is 2.5 and 1.7°C lower than observations in 1935 and 1957 respectively (Figures 6a and 6b), suggesting a transient negative effect even on the QWA metrics that are otherwise positive temperature responders at this location in response to the extreme conditions in 1934 and 1956. Both bristlecone pine species, *P. longaeva* and *P. aristata*, are known to have high year-to-year autocorrelation in total ring width, often interpreted as "biological memory," where antecedent climate conditions affect the current year of growth (Bale et al., 2011; LaMarche Jr & Stockton, 1974; Millar et al., 2015). This biological memory is likely partially driven by the previous years' storage and re-mobilization of non-structural carbohydrates (Peltier et al., 2022). The extreme drought years may have led to low carbon availability, hindering the allocation of sufficient carbon to latewood formation in the following year, resulting in lower aMXD/MxRCWT (Anderegg et al., 2015; Huang et al., 2018; Kannenberg et al., 2022; Peltier et al., 2022).

The analysis of a pluvial period offers a contrasting perspective on hydroclimate variability recorded at our sites. The 1980s' pluvial was a multi-year period of anomalously wet conditions in SWNA associated with El Niño conditions (Fye et al., 2004) and anomalously wet summer monsoon rainfall (Kim, 2002; Ziaco et al., 2020). Although observational August/September maximum temperature over this timeframe is 0.5°C below the 1917–2017 average, this is not reflected in the LCH aMXD/MxRCWT (Figure 6c), suggesting a potential disconnect or threshold behavior in the response of these proxy data during anomalous pluvial conditions. Observing above-normal growth in conifers on the Colorado Plateau after the 1815 Tambora eruption, Cleaveland (1992) postulated that the reduced moisture stress from lower temperature and/or increased precipitation (attributed to the eruption) led to a delayed onset of seasonal drought-induced dormancy, favoring increased development of the latewood density. We can also perhaps observe the inverse of this effect in the 2011/2012 drought years, where an earlier drought induced dormancy would cause the aMXD/MxRCWT to either not capture the full magnitude of August/September temperature or have a negative growth response to increased temperature. Although the observational August/September maximum temperature is 1.7 and 1.5°C above the 1917–2017 average in 2011 and 2012 respectively, the aMXD/MxRCWT predictors do not track increasing temperature throughout the 2010s (Figure 6d).

This observed divergence and the decline in correlation between observed and proxy scaled August/September maximum temperature and aMXD/MXrCWT during the 1967–2017 period (Table 2), prompts questions about the effect of rising temperatures on tree growth dynamics in previously temperature-limited environments and the apparent increase in moisture sensitivity at high elevation sites (Bunn et al., 2018). The focus of this paper is not explicitly on this temperature sensitivity decline and initial investigations thus far remain inconclusive as to the exact mechanism. It could be that steadily increasing temperatures are causing LCH to transition into a state more closely resembling lower elevation conditions like LCL. It is also possible we are observing the effect of rising vapor pressure deficit, which has been shown to confound climate-growth responses in Great Basin bristlecone pine (de Boer et al., 2019). This apparent loss of sensitivity in latewood-related chronologies at high elevations calls for further research into the intricate connections between temperature changes, atmospheric moisture availability, and the stability of the tree-ring proxy response. In a future drier climate, *Pinus aristata* productivity and carbon uptake may increasingly decouple from radial growth because of drought-induced allocation of carbon away from radial growth (Kannenberg et al., 2022).

## 5. Conclusion

This study investigates the differences in the response of tree growth and xylogenesis to climatic variables at two sites at different elevations, LCL and LCH, using QWA. We find distinct climate signals at the two sites, consistent with the patterns identified by Salzer et al. (2009) of tree-growth-climate relationship changes across an elevation gradient in Southwestern North America. At LCL, the growth patterns and cellular characteristics are primarily controlled by moisture availability, typical of lower elevation forest zones, whereas at LCH, tree growth exhibits a mixed climate response including correlations between cellular characteristics and temperature, indicative of thermal limitations at higher elevations.

We further examine sub-seasonal responsiveness of QWA versus TRW measurements. We find that the early-wood lumen area is more responsive to environmental changes compared to total TRW. This responsiveness is particularly evident during periods of extreme drought. Our findings also underscore the utility of QWA in distinguishing between different drought conditions and seasonality. By analyzing multiple aspects of wood anatomy, we gain insights into the physiological responses of trees to varying droughts. This analysis also provides a nuanced perspective on how *P. aristata* at different elevations respond to the same climatic extremes. Future research could compare QWA data with microdensitometric and blue intensity measurements to further expand dendroclimatic proxies from *P. aristata* and assess their potential for climate reconstructions.

Our efforts to identify a temperature signal from using wood anatomical data reveal an apparent interaction between rising temperatures and drought stress and a decline in temperature sensitivity at higher elevations. This divergence indicates a shift in the climatic drivers of tree-ring formation and an evolving climate-growth relationship. The complexity of the climate-growth relationship at Little Costilla Peak is likely in part because of the site location at the margin of the species' range, which offers the chance to detect shifts in limiting factors. Although this is not ideal for reconstructions at this site, it does give us the opportunity to evaluate what is possible with an additional proxy-data approach like QWA. Our findings underscore the necessity for continued research into the effects of increasing temperatures on tree physiology and highlight the value of integrating QWA data with traditional dendrochronological methods to better understand these complex dynamics.

## Data Availability Statement

The tree-ring data generated as part of this study, and the code used to perform data analysis and to produce the manuscript's figures are published on Zenodo (Edwards et al., 2024). All climate data sets used in this study and their sources are listed below: CRU TS Version 4.06 (Harris et al., 2020, 2022), Global SPEI database (Beguería et al., 2014, 2020), Topography Weather (TopoWx) daily climate data (Oyler et al., 2016, 2017), and Red River Pass SNOTEL site data (USDA Natural Resources Conservation Service, 2024).

**Acknowledgments**
CW, WT, and JE were supported by NSF P2C2 grant AGS-1702271. JE and KJA were additionally supported by NSF P2C2 grant AGS-2102993. GvA received funding from the SNF project XELLCLIM (no.200021_182398). The authors thank Kyler McNeely and Zanubia Sethuraju for lab assistance.

## References

Anderegg, W. R., Schwalm, C., Biondi, F., Camarero, J. J., Koch, G., Litvak, M., et al. (2015). Pervasive drought legacies in forest ecosystems and their implications for carbon cycle models. *Science*, *349*(6247), 528–532. https://doi.org/10.1126/science.aab1833

Bailey, K., Szejner, P., Strange, B., Monson, R., & Hu, J. (2023). The influence of winter snowpack on the use of summer rains in montane pine forests across the southwest US. *Journal of Geophysical Research: Biogeosciences*, *128*(9), e2023JG007494. https://doi.org/10.1029/2023jg007494

Balanzategui, D., Nordhauß, H., Heinrich, I., Biondi, F., Miley, N., Hurley, A. G., & Ziaco, E. (2021). Wood anatomy of Douglas-fir in Eastern Arizona and its relationship with Pacific Basin climate. *Frontiers in Plant Science*, *12*, 702442. https://doi.org/10.3389/fpls.2021.702442

Bale, R. J., Robertson, I., Salzer, M. W., Loader, N. J., Leavitt, S. W., Gagen, M., et al. (2011). An annually resolved bristlecone pine carbon isotope chronology for the last millennium. *Quaternary Research*, *76*(1), 22–29. https://doi.org/10.1016/j.yqres.2011.05.004

Beguería, S., Vicente-Serrano, S. M., Reig, F., & Latorre, B. (2014). Standardized precipitation evapotranspiration index (SPEI) revisited: Parameter fitting, evapotranspiration models, tools, datasets and drought monitoring. *International Journal of Climatology*, *34*(10), 3001–3023. https://doi.org/10.1002/joc.3887

Beguería, S., Vicente-Serrano, S. M., Reig, F., & Latorre, B. (2020). SPEIbase (version 2.6) [Dataset]. *DIGITAL.CSIC*. https://doi.org/10.20350/digitalCSIC/15555

Björklund, J., Fonti, M. V., Fonti, P., Van den Bulcke, J., & von Arx, G. (2021). Cell wall dimensions reign supreme: Cell wall composition is irrelevant for the temperature signal of latewood density/blue intensity in Scots pine. *Dendrochronologia*, *65*, 125785. https://doi.org/10.1016/j.dendro.2020.125785

Björklund, J., Seftigen, K., Fonti, P., Nievergelt, D., & von Arx, G. (2020). Dendroclimatic potential of dendroanatomy in temperature-sensitive *Pinus sylvestris*. *Dendrochronologia*, *60*, 125673. https://doi.org/10.1016/j.dendro.2020.125673

Bruening, J. M., Tran, T. J., Bunn, A. G., Weiss, S. B., & Salzer, M. W. (2017). Fine-scale modeling of bristlecone pine treeline position in the Great Basin, USA. *Environmental Research Letters*, *12*(1), 014008. https://doi.org/10.1088/1748-9326/aa5432

Bunn, A. G. (2008). A dendrochronology program library in R (dplR). *Dendrochronologia*, *26*(2), 115–124. https://doi.org/10.1016/j.dendro.2008.01.002

Bunn, A. G., Hughes, M. K., & Salzer, M. W. (2011). Topographically modified tree-ring chronologies as a potential means to improve paleoclimate inference. *Climatic Change*, *105*(3), 627–634. https://doi.org/10.1007/s10584-010-0005-5

Bunn, A. G., Salzer, M. W., Anchukaitis, K. J., Bruening, J. M., & Hughes, M. K. (2018). Spatiotemporal variability in the climate growth response of high elevation bristlecone pine in the White Mountains of California. *Geophysical Research Letters*, *45*(24), 13,312–13,321. https://doi.org/10.1029/2018gl080981

Buttò, V., Deslauriers, A., Rossi, S., Rozenberg, P., Shishov, V., & Morin, H. (2020). The role of plant hormones in tree-ring formation. *Trees*, *34*(2), 315–335. https://doi.org/10.1007/s00468-019-01940-4

Cabon, A., Fernández-de Uña, L., Gea-Izquierdo, G., Meinzer, F. C., Woodruff, D. R., Martínez-Vilalta, J., & De Cáceres, M. (2020). Water potential control of turgor-driven tracheid enlargement in Scots pine at its xeric distribution edge. *New Phytologist*, *225*(1), 209–221. https://doi.org/10.1111/nph.16146

Carrer, M., Castagneri, D., Prendin, A. L., Petit, G., & von Arx, G. (2017). Retrospective analysis of wood anatomical traits reveals a recent extension in tree cambial activity in two high-elevation conifers. *Frontiers in Plant Science*, *8*, 737. https://doi.org/10.3389/fpls.2017.00737

Castagneri, D., Fonti, P., von Arx, G., & Carrer, M. (2017). How does climate influence xylem morphogenesis over the growing season? Insights from long-term intra-ring anatomy in *Picea abies*. *Annals of Botany*, *119*(6), 1011–1020. https://doi.org/10.1093/aob/mcw274

Castagneri, D., Petit, G., & Carrer, M. (2015). Divergent climate response on hydraulic-related xylem anatomical traits of Picea abies along a 900-m altitudinal gradient. *Tree Physiology*, *35*(12), 1378–1387. https://doi.org/10.1093/treephys/tpv085

Cleaveland, M. K. (1992). *Volcanic effects on Colorado plateau Douglas-Fir tree rings*. Canadian Museum of Nature.

Cook, B. I., Mankin, J. S., Marvel, K., Williams, A. P., Smerdon, J. E., & Anchukaitis, K. J. (2020). Twenty-first century drought projections in the CMIP6 forcing scenarios. *Earth's Future*, *8*(6), e2019EF001461. https://doi.org/10.1029/2019ef001461

Cook, B. I., Mankin, J. S., Williams, A. P., Marvel, K. D., Smerdon, J. E., & Liu, H. (2021). Uncertainties, limits, and benefits of climate change mitigation for soil moisture drought in southwestern North America. *Earth's Future*, *9*(9), e2021EF002014. https://doi.org/10.1029/2021ef002014

Cook, B. I., Miller, R. L., & Seager, R. (2009). Amplification of the North American "Dust Bowl" drought through human-induced land degradation. *Proceedings of the National Academy of Sciences*, *106*(13), 4997–5001. https://doi.org/10.1073/pnas.0810200106

Cook, B. I., Seager, R., & Smerdon, J. E. (2014). The worst North American drought year of the last millennium: 1934. *Geophysical Research Letters*, *41*(20), 7298–7305. https://doi.org/10.1002/2014gl061661

Cook, E. R., Krusic, P., Peters, K., & Holmes, R. (2017). Program ARSTAN version48d2: Autoregressive tree-ring standardization program. *Tree-Ring Laboratory of LDEO*.

Cook, E. R., Seager, R., Cane, M. A., & Stahle, D. W. (2007). North American drought: Reconstructions, causes, and consequences. *Earth-Science Reviews*, *81*(1–2), 93–134. https://doi.org/10.1016/j.earscirev.2006.12.002

Cook, E. R., Seager, R., Heim Jr, R. R., Vose, R. S., Herweijer, C., & Woodhouse, C. (2010). Megadroughts in North America: Placing IPCC projections of hydroclimatic change in a long-term palaeoclimate context. *Journal of Quaternary Science*, *25*(1), 48–61. https://doi.org/10.1002/jqs.1303

Cook, E. R., Woodhouse, C. A., Eakin, C. M., Meko, D. M., & Stahle, D. (2004). Long-term aridity changes in the western United States. *Science*, *306*(5698), 1015–1018. https://doi.org/10.1126/science.1102586

Coulthard, B. L., Anchukaitis, K. J., Pederson, G. T., Cook, E., Littell, J., & Smith, D. J. (2021). Snowpack signals in North American tree rings. *Environmental Research Letters*, *16*(3), 034037. https://doi.org/10.1088/1748-9326/abd5de

Cuny, H. E., Fonti, P., Rathgeber, C. B., von Arx, G., Peters, R. L., & Frank, D. C. (2019). Couplings in cell differentiation kinetics mitigate air temperature influence on conifer wood anatomy. *Plant, Cell and Environment*, *42*(4), 1222–1232. https://doi.org/10.1111/pce.13464

Cuny, H. E., & Rathgeber, C. B. (2016). Xylogenesis: Coniferous trees of temperate forests are listening to the climate tale during the growing season but only remember the last words. *Plant Physiology*, *171*(1), 306–317. https://doi.org/10.1104/pp.16.00037

Cuny, H. E., Rathgeber, C. B. K., Frank, D., Fonti, P., & Fournier, M. (2014). Kinetics of tracheid development explain conifer tree-ring structure. *New Phytologist*, *203*(4), 1231–1241. https://doi.org/10.1111/nph.12871

D'Arrigo, R. D., & Jacoby, G. C. (1991). A 1000-year record of winter precipitation from northwestern New Mexico, USA: A reconstruction from tree-rings and its relation to El Niño and the Southern Oscillation. *The Holocene*, *1*(2), 95–101. https://doi.org/10.1177/095968369100100201

Das, T., Pierce, D. W., Cayan, D. R., Vano, J. A., & Lettenmaier, D. P. (2011). The importance of warm season warming to western US streamflow changes. *Geophysical Research Letters*, *38*(23). https://doi.org/10.1029/2011gl049660

de Boer, H. J., Robertson, I., Clisby, R., Loader, N. J., Gagen, M., Young, G. H., et al. (2019). Tree-ring isotopes suggest atmospheric drying limits temperature–growth responses of treeline bristlecone pine. *Tree Physiology*, *39*(6), 983–999. https://doi.org/10.1093/treephys/tpz018

Denne, M. (1989). Definition of latewood according to Mork (1928). *IAWA Journal*, *10*(1), 59–62. https://doi.org/10.1163/22941932-90001112

Edwards, J., Tintor, W. L., Nolin, A. F., Woodhouse, C. A., von Arx, G., & Anchukaitis, K. J. (2024). Multiple elevation-dependent climate signals from quantitative wood anatomical measurements of Rocky Mountain bristlecone pine (Version 1.0) [Software]. *Zenodo*. https://doi.org/10.5281/zenodo.13975858

Fonti, P., von Arx, G., García-González, I., Eilmann, B., Sass-Klaassen, U., Gärtner, H., & Eckstein, D. (2010). Studying global change through investigation of the plastic responses of xylem anatomy in tree rings. *New Phytologist*, *185*(1), 42–53. https://doi.org/10.1111/j.1469-8137.2009.03030.x

Fritts, H. C. (1974). Relationships of ring widths in arid-site conifers to variations in monthly temperature and precipitation. *Ecological Monographs*, *44*(4), 411–440. https://doi.org/10.2307/1942448

Fritts, H. C. (1976). *Tree rings and climate*. Academic Press.

Fye, F. K., Stahle, D. W., & Cook, E. R. (2004). Twentieth-century sea surface temperature patterns in the Pacific during decadal moisture regimes over the United States. *Earth Interactions*, *8*(22), 1–22. https://doi.org/10.1175/1087-3562(2004)8<1:tsstpi>2.0.co;2

Gangopadhyay, S., Woodhouse, C. A., McCabe, G. J., Routson, C. C., & Meko, D. M. (2022). Tree rings reveal unmatched 2nd century drought in the Colorado River Basin. *Geophysical Research Letters*, *49*(11), e2022GL098781. https://doi.org/10.1029/2022gl098781

Gärtner, H., & Schweingruber, F. (2013). *Microscopic preparation techniques for plant stem analysis* (Vol. 34). Kessel Publishing House.

Gleason, S. M., Westoby, M., Jansen, S., Choat, B., Hacke, U. G., Pratt, R. B., et al. (2016). Weak tradeoff between xylem safety and xylem-specific hydraulic efficiency across the world's woody plant species. *New Phytologist*, *209*(1), 123–136. https://doi.org/10.1111/nph.13646

González-Cásares, M., Camarero, J. J., Colangelo, M., Rita, A., & Pompa-García, M. (2019). High responsiveness of wood anatomy to water availability and drought near the equatorial rear edge of Douglas-fir. *Canadian Journal of Forest Research*, *49*(9), 1114–1123. https://doi.org/10.1139/cjfr-2019-0120

Griffin, D., & Anchukaitis, K. J. (2014). How unusual is the 2012–2014 California drought? *Geophysical Research Letters*, *41*(24), 9017–9023. https://doi.org/10.1002/2014gl062433

Griffin, D., Woodhouse, C. A., Meko, D. M., Stahle, D. W., Faulstich, H. L., Carrillo, C., et al. (2013). North American monsoon precipitation reconstructed from tree-ring latewood. *Geophysical Research Letters*, *40*(5), 954–958. https://doi.org/10.1002/grl.50184

Grigg, N. S. (2014). The 2011–2012 drought in the United States: New lessons from a record event. *International Journal of Water Resources Development*, *30*(2), 183–199. https://doi.org/10.1080/07900627.2013.847710

Gruber, A., Baumgartner, D., Zimmermann, J., & Oberhuber, W. (2009). Temporal dynamic of wood formation in *Pinus cembra* along the alpine treeline ecotone and the effect of climate variables. *Trees*, *23*(3), 623–635. https://doi.org/10.1007/s00468-008-0307-7

Guérin, M., Von Arx, G., Martin-Benito, D., Andreu-Hayles, L., Griffin, K. L., McDowell, N. G., et al. (2020). Distinct xylem responses to acute vs prolonged drought in pine trees. *Tree Physiology*, *40*(5), 605–620. https://doi.org/10.1093/treephys/tpz144

Hacke, U. G., & Sperry, J. S. (2001). Functional and ecological xylem anatomy. *Perspectives in Plant Ecology, Evolution and Systematics*, *4*(2), 97–115. https://doi.org/10.1078/1433-8319-00017

Hacke, U. G., Sperry, J. S., Pockman, W. T., Davis, S. D., & McCulloh, K. A. (2001). Trends in wood density and structure are linked to prevention of xylem implosion by negative pressure. *Oecologia*, *126*(4), 457–461. https://doi.org/10.1007/s004420100628

Han, R.-Y., Gong, X.-W., Li, M.-Y., Leng, Q.-N., Zhou, Y.-J., Ning, Q.-R., & Hao, G.-Y. (2023). Combined tree-ring width and wood anatomy chronologies provide insights into the radial growth and hydraulic strategies in response to an extreme drought in plantation-grown Mongolian pine trees. *Environmental and Experimental Botany*, *208*, 105259. https://doi.org/10.1016/j.envexpbot.2023.105259

Harris, I., Osborn, T. J., Jones, P., & Lister, D. (2020). Version 4 of the CRU TS monthly high-resolution gridded multivariate climate dataset. *Scientific Data*, *7*(1), 109. https://doi.org/10.1038/s41597-020-0453-3

Harris, I., Osborn, T. J., Jones, P., & Lister, D. (2022). CRU TS (version 4.06) [Dataset]. https://crudata.uea.ac.uk/cru/data/hrg/cru_ts_4.06/

Heeter, K. J., Harley, G. L., Maxwell, J. T., Wilson, R. J., Abatzoglou, J. T., Rayback, S. A., et al. (2021). Summer temperature variability since 1730 CE across the low-to-mid latitudes of western North America from a tree ring blue intensity network. *Quaternary Science Reviews*, *267*, 107064. https://doi.org/10.1016/j.quascirev.2021.107064

Hoch, G., & Körner, C. (2012). Global patterns of mobile carbon stores in trees at the high-elevation tree line. *Global Ecology and Biogeography*, *21*(8), 861–871. https://doi.org/10.1111/j.1466-8238.2011.00731.x

Huang, M., Wang, X., Keenan, T. F., & Piao, S. (2018). Drought timing influences the legacy of tree growth recovery. *Global Change Biology*, *24*(8), 3546–3559. https://doi.org/10.1111/gcb.14294

Jones, P. D., & Mann, M. E. (2004). Climate over past millennia. *Reviews of Geophysics*, *42*(2). https://doi.org/10.1029/2003rg000143

Jost, G., Weiler, M., Gluns, D. R., & Alila, Y. (2007). The influence of forest and topography on snow accumulation and melt at the watershed-scale. *Journal of Hydrology*, *347*(1–2), 101–115. https://doi.org/10.1016/j.jhydrol.2007.09.006

Kannenberg, S. A., Cabon, A., Babst, F., Belmecheri, S., Delpierre, N., Guerrieri, R., et al. (2022). Drought-induced decoupling between carbon uptake and tree growth impacts forest carbon turnover time. *Agricultural and Forest Meteorology*, *322*, 108996. https://doi.org/10.1016/j.agrformet.2022.108996

Kim, J. (2002). Precipitation variability associated with the North American Monsoon in the 20th century. *Geophysical Research Letters*, *29*(13), 28-1–28-4. https://doi.org/10.1029/2001gl014316

King, K. E., Cook, E. R., Anchukaitis, K. J., Cook, B. I., Smerdon, J. E., Seager, R., et al. (2024). Increasing prevalence of hot drought across western North America since the 16th century. *Science Advances*, *10*(4). https://doi.org/10.1126/sciadv.adj4289

LaMarche Jr, V. C., & Stockton, C. W. (1974). Chronologies from termperature-sensitive bristlecone pines at upper treeline in Western United States. *Tree-Ring Bulletin*, *34*, 21–44.

Lauder, J. D., Moran, E. V., & Hart, S. C. (2019). Fight or flight? Potential tradeoffs between drought defense and reproduction in conifers. *Tree Physiology*, *39*(7), 1071–1085. https://doi.org/10.1093/treephys/tpz031

Mankin, J., Simpson, I., Hoell, A., Fu, R., Lisonbee, J., Sheffield, A., & Barrie, D. (2021). NOAA drought task force report on the 2020–2021 southwestern US drought.

Martin-Benito, D., Beeckman, H., & Canellas, I. (2013). Influence of drought on tree rings and tracheid features of *Pinus nigra* and *Pinus sylvestris* in a mesic Mediterranean forest. *European Journal of Forest Research*, *132*(1), 33–45. https://doi.org/10.1007/s10342-012-0652-3

Marvel, K., Su, W., Delgado, R., Aarons, S., Chatterjee, A., Garcia, M. E., et al. (2023). Climate trends [Book Section]. In A. Crimmins, C. Avery, D. Easterling, K. Kunkel, B. Stewart, & T. Maycock (Eds.), *Fifth National Climate Assessment (chap. 2)*. U.S. Global Change Research Program. https://doi.org/10.7930/NCA5.2023.CH2

McGregor, K. M. (1985). Drought during the 1930s and 1950s in the central United States. *Physical Geography*, *6*(3), 288–301. https://doi.org/10.1080/02723646.1985.10642277

Meko, D. M., & Woodhouse, C. A. (2011). Application of streamflow reconstruction to water resources management. In *Dendroclimatology: Progress and prospects* (pp. 231–261).

Meko, D. M., Woodhouse, C. A., Baisan, C. A., Knight, T., Lukas, J. J., Hughes, M. K., & Salzer, M. W. (2007). Medieval drought in the upper Colorado River Basin. *Geophysical Research Letters*, *34*(10), L10705. https://doi.org/10.1029/2007GL029988

Millar, C. I., Westfall, R. D., Delany, D. L., Flint, A. L., & Flint, L. E. (2015). Recruitment patterns and growth of high-elevation pines in response to climatic variability (1883–2013), in the western Great Basin, USA. *Canadian Journal of Forest Research*, *45*(10), 1299–1312. https://doi.org/10.1139/cjfr-2015-0025

Milly, P. C., & Dunne, K. A. (2020). Colorado River flow dwindles as warming-driven loss of reflective snow energizes evaporation. *Science*, *367*(6483), 1252–1255. https://doi.org/10.1126/science.aay9187

Mork, E. (1928). Die qualität dês fichtenholzes unter besonderer rucksichtnahme auf Schleif-und Papierholz. *Papier-fabrikant*, *26*, 741–747.

Olano, J. M., Eugenio, M., Garcia-Cervigon, A. I., Folch, M., & Rozas, V. (2012). Quantitative tracheid anatomy reveals a complex environmental control of wood structure in continental Mediterranean climate. *International Journal of Plant Sciences*, *173*(2), 137–149. https://doi.org/10.1086/663165

Ols, C., Klesse, S., Girardin, M. P., Evans, M. E., DeRose, R. J., & Trouet, V. (2023). Detrending climate data prior to climate–growth analyses in dendroecology: A common best practice? *Dendrochronologia*, *79*, 126094. https://doi.org/10.1016/j.dendro.2023.126094

Oyler, J. W., Dobrowski, S. Z., Holden, Z. A., & Running, S. W. (2016). Remotely sensed land skin temperature as a spatial predictor of air temperature across the conterminous United States. *Journal of Applied Meteorology and Climatology*, *55*(7), 1441–1457. https://doi.org/10.1175/jamc-d-15-0276.1

Oyler, J. W., Dobrowski, S. Z., Holden, Z. A., & Running, S. W. (2017). TopoWx (version 1) [Dataset]. https://www.scrim.psu.edu/resources/topowx/

Peltier, D. M., Guo, J., Nguyen, P., Bangs, M., Wilson, M., Samuels-Crow, K., et al. (2022). Temperature memory and non-structural carbohydrates mediate legacies of a hot drought in trees across the southwestern USA. *Tree Physiology*, *42*(1), 71–85. https://doi.org/10.1093/treephys/tpab091

Peters, R. L., Steppe, K., Cuny, H. E., De Pauw, D. J., Frank, D. C., Schaub, M., et al. (2021). Turgor–a limiting factor for radial growth in mature conifers along an elevational gradient. *New Phytologist*, *229*(1), 213–229. https://doi.org/10.1111/nph.16872

Pittermann, J., Sperry, J. S., Wheeler, J. K., Hacke, U. G., & Sikkema, E. H. (2006). Mechanical reinforcement of tracheids compromises the hydraulic efficiency of conifer xylem. *Plant, Cell and Environment*, *29*(8), 1618–1628. https://doi.org/10.1111/j.1365-3040.2006.01539.x

Prendin, A. L., Petit, G., Carrer, M., Fonti, P., Björklund, J., & von Arx, G. (2017). New research perspectives from a novel approach to quantify tracheid wall thickness. *Tree Physiology*, *37*(7), 976–983. https://doi.org/10.1093/treephys/tpx037

Rathgeber, C. B., Cuny, H. E., & Fonti, P. (2016). Biological basis of tree-ring formation: A crash course. *Frontiers in Plant Science*, *7*, 734. https://doi.org/10.3389/fpls.2016.00734

Richman, M. B. (1986). Rotation of principal components. *Journal of Climatology*, *6*(3), 293–335. https://doi.org/10.1002/joc.3370060305

Routson, C. C., Woodhouse, C. A., & Overpeck, J. T. (2011). Second century megadrought in the Rio Grande headwaters, Colorado: How unusual was medieval drought? *Geophysical Research Letters*, *38*(22). https://doi.org/10.1029/2011gl050015

Salzer, M. W., Hughes, M. K., Bunn, A. G., & Kipfmueller, K. F. (2009). Recent unprecedented tree-ring growth in bristlecone pine at the highest elevations and possible causes. *Proceedings of the National Academy of Sciences of the United States of America*, *106*(48), 20348–20353. https://doi.org/10.1073/pnas.0903029106

Salzer, M. W., & Kipfmueller, K. F. (2005). Reconstructed temperature and precipitation on a millennial timescale from tree-rings in the southern Colorado Plateau, USA. *Climatic Change*, *70*(3), 465–487. https://doi.org/10.1007/s10584-005-5922-3

Salzer, M. W., Larson, E. R., Bunn, A. G., & Hughes, M. K. (2014). Changing climate response in near-treeline bristlecone pine with elevation and aspect. *Environmental Research Letters*, *9*(11), 114007. https://doi.org/10.1088/1748-9326/9/11/114007

Salzer, M. W., Pearson, C. L., & Baisan, C. H. (2019). Dating the methuselah walk bristlecone pine floating chronologies. *Tree-Ring Research*, *75*(1), 61–66. https://doi.org/10.3959/1536-1098-75.1.61

Schoettle, A. W., & Coop, J. D. (2017). Range-wide conservation of *Pinus aristata*: A genetic collection with ecological context for proactive management today and resources for tomorrow. *New Forests*, *48*(2), 181–199. https://doi.org/10.1007/s11056-017-9570-z

Seftigen, K., Fonti, M. V., Luckman, B., Rydval, M., Stridbeck, P., Von Arx, G., et al. (2022). Prospects for dendroanatomy in paleoclimatology–a case study on *Picea engelmannii* from the Canadian Rockies. *Climate of the Past Discussions*, *2022*(5), 1–32. https://doi.org/10.5194/cp-18-1151-2022

Stahle, D. W., Cook, E. R., Burnette, D. J., Villanueva, J., Cerano, J., Burns, J. N., et al. (2016). The Mexican Drought Atlas: Tree-ring reconstructions of the soil moisture balance during the late pre-Hispanic, colonial, and modern eras. *Quaternary Science Reviews*, *149*, 34–60. https://doi.org/10.1016/j.quascirev.2016.06.018

Tintor, W. L., & Woodhouse, C. A. (2021). The variable climate response of Rocky Mountain bristlecone pine (*Pinus aristata* Engelm.). *Dendrochronologia*, *68*, 125846. https://doi.org/10.1016/j.dendro.2021.125846

Tran, T. J., Bruening, J. M., Bunn, A. G., Salzer, M. W., & Weiss, S. B. (2017). Cluster analysis and topoclimate modeling to examine bristlecone pine tree-ring growth signals in the Great Basin, USA. *Environmental Research Letters*, *12*(1), 014007. https://doi.org/10.1088/1748-9326/aa5388

Udall, B., & Overpeck, J. (2017). The twenty-first century Colorado River hot drought and implications for the future. *Water Resources Research*, *53*(3), 2404–2418. https://doi.org/10.1002/2016wr019638

USDA Natural Resources Conservation Service. (2024). SNOTEL data: Red River Pass #2–Site 715, New Mexico [Dataset]. https://wcc.sc.egov.usda.gov/nwcc/site?sitenum=715

Vaganov, E. A., Anchukaitis, K. J., & Evans, M. N. (2011). How well understood are the processes that create dendroclimatic records? A mechanistic model of the climatic control on conifer tree-ring growth dynamics. *Dendroclimatology: Progress and Prospects*, 37–75. https://doi.org/10.1007/978-1-4020-5725-0_3

Vaganov, E. A., Hughes, M. K., & Shashkin, A. V. (2006). *Growth dynamics of conifer tree rings: Images of past and future environments* (Vol. 183). Springer Science & Business Media.

von Arx, G., & Carrer, M. (2014). ROXAS – A new tool to build centuries-long tracheid-lumen chronologies in conifers. *Dendrochronologia*, *32*(3), 290–293. https://doi.org/10.1016/j.dendro.2013.12.001

von Arx, G., Crivellaro, A., Prendin, A. L., Čufar, K., & Carrer, M. (2016). Quantitative wood anatomy—Practical guidelines. *Frontiers in Plant Science*, *7*. https://doi.org/10.3389/fpls.2016.00781

Vose, R., Easterling, D. R., Kunkel, K., LeGrande, A., & Wehner, M. (2017). Temperature changes in the United States. In *Climate science special report: Fourth national climate assessment* (Vol. 1). (GSFC-E-DAA-TN49028).

Weiss, J. L., Castro, C. L., & Overpeck, J. T. (2009). Distinguishing pronounced droughts in the southwestern United States: Seasonality and effects of warmer temperatures. *Journal of Climate*, *22*(22), 5918–5932. https://doi.org/10.1175/2009jcli2905.1

Wigley, T. M. L., Briffa, K. R., & Jones, P. D. (1984). On the average value of correlated time series, with applications in dendroclimatology and hydrometeorology. *Journal of Climate and Applied Meteorology*, *23*(2), 201–213. https://doi.org/10.1175/1520-0450(1984)023<0201:otavoc>2.0.co;2

Wiken, E., Nava, F. J., & Griffith, G. (2011). *North American terrestrial ecoregions—level III* (p. 149). Commission for Environmental Cooperation.

Williams, A. P., Cook, B. I., & Smerdon, J. E. (2022). Rapid intensification of the emerging southwestern North American megadrought in 2020–2021. *Nature Climate Change*, *12*(3), 232–234. https://doi.org/10.1038/s41558-022-01290-z

Williams, A. P., Cook, E. R., Smerdon, J. E., Cook, B. I., Abatzoglou, J. T., Bolles, K., et al. (2020). Large contribution from anthropogenic warming to an emerging North American megadrought. *Science*, *368*(6488), 314–318. https://doi.org/10.1126/science.aaz9600

Woodhouse, C. A., Gray, S. T., & Meko, D. M. (2006). Updated streamflow reconstructions for the Upper Colorado River basin. *Water Resources Research*, *42*(W05415). https://doi.org/10.1029/2005wr004455

Woodhouse, C. A., Pederson, G. T., & Gray, S. T. (2011). An 1800-yr record of decadal-scale hydroclimatic variability in the upper Arkansas River basin from bristlecone pine. *Quaternary Research*, *75*(3), 483–490. https://doi.org/10.1016/j.yqres.2010.12.007

Woodhouse, C. A., Pederson, G. T., Morino, K., McAfee, S. A., & McCabe, G. J. (2016). Increasing influence of air temperature on upper Colorado River streamflow. *Geophysical Research Letters*, *43*(5), 2174–2181. https://doi.org/10.1002/2015gl067613

Woodhouse, C. A., Stahle, D. W., & Díaz, J. V. (2012). Rio Grande and Rio Conchos water supply variability over the past 500 years. *Climate Research*, *51*(2), 147–158. https://doi.org/10.3354/cr01059

Ziaco, E., Biondi, F., & Heinrich, I. (2016). Wood cellular dendroclimatology: Testing new proxies in Great Basin bristlecone pine. *Frontiers in Plant Science*, *7*, 1602. https://doi.org/10.3389/fpls.2016.01602

Ziaco, E., Biondi, F., Rossi, S., & Deslauriers, A. (2016). Environmental drivers of cambial phenology in Great Basin bristlecone pine. *Tree Physiology*, *36*(7), 818–831. https://doi.org/10.1093/treephys/tpw006

Ziaco, E., Miley, N., & Biondi, F. (2020). Reconstruction of seasonal and water-year precipitation anomalies from tree-ring records of the southwestern United States. *Palaeogeography, Palaeoclimatology, Palaeoecology*, *547*, 109689. https://doi.org/10.1016/j.palaeo.2020.109689